Effective thermal resistance of a photonic crystal microcavity

L.-D. Haret, A. Ghrib, X. Checoury, N. Cazier, Z. Han, M. El Kurdi, S. Sauvage, and P. Boucaud*

Institut d'Electronique Fondamentale, CNRS—Univ. Paris Sud 11, Bâtiment 220, F-91405 Orsay, France
Corresponding author: philippe.boucaud@ief.u-psud.fr

We present a simple method to accurately measure the effective thermal resistance of a photonic crystal microcavity. The cavity is embedded between two Schottky contacts forming a metal-semiconductor-metal device. The photocarriers circulating in the device provide a local temperature rise that can be dominated by Joule effect under certain conditions. We show that the effective thermal resistance (R_{th}) can be experimentally deduced from the spectral shift of the cavity resonance wavelength measured at different applied bias. We deduce a value of $R_{\mathrm{th}} = 1.6 \times 10^4 \ \mathrm{KW}^{-1}$ for a microcavity on silicon-on-insulator, which is in good agreement with 3D thermal modeling by finite elements.   © 2014 Optical Society of America

Photonic crystal microcavities can exhibit high-quality factors and small modal volumes. These features lead to reinforcement of nonlinear interactions. Numerous nonlinear properties based on second-order or third-order nonlinear susceptibilities have thus been investigated in recent years with photonic crystal cavities [1–3]. Nonlinear nanophotonics presents a strong interest for the study of the intrinsic properties of the cavities as well as for the integration of nanodevices into photonic circuits. One of the consequence of the high-quality factors [4,5] is the large optical energy that can be localized in small mode volumes. This feature enhances the nonlinear response, but it also leads to significant thermal heating of the cavities. This effect is even reinforced in membrane-type photonic crystal devices, which exhibit lower thermal dissipation as compared to nonsuspended structures. Thermal heating leads to change in the refractive index through thermo-optic coefficient and shifts the resonance wavelength of the cavities and is, in most cases, considered a negative side effect for nonlinear nanophotonics. The weak thermal dissipation can, for example, limit the operation of membrane-type photonic crystal lasers [6]. It has also a major impact for the operation of a photonic crystal Raman laser [7] and more generally for the operation conditions of nonlinear devices [8].

The thermal properties of cavities can be described by the effective thermal resistance R_{th} in units of Kelvins per Watt that represents the ratio between the temperature rise ΔT and the power P provided to the structure, either optically or electrically. This value traduces the capacity of a structure to resist heat flow. The effective thermal resistance of a cavity can be estimated by finite element modeling [9] or by a combination of measurements involving the spectral shift of the resonance wavelength and the power transmitted through the cavity as a function of input power [10,11]. One difficulty that generally arises for this determination is the exact knowledge of the absorbed optical power either by linear absorption, two-photon absorption, or free carrier absorption. Moreover, the locally absorbed and dissipated optical power depends on the free carrier lifetime in the cavity, which is usually unknown or at least not precisely known because of carrier diffusion and nonradiative recombinations at the interfaces. The experimental measurement of the thermal resistance in small mode volume photonic crystal cavities is thus a difficult task.

In this Letter, we show that the effective thermal resistance of a photonic crystal microcavity can be determined by implementing two Schottky contacts in close proximity of the cavity. The free carriers optically generated in the cavity are collected by the Schottky electrodes such as in a metal-semiconductor-metal detector. Instead of trying to evaluate accurately the optical power locally absorbed and dissipated, we control the thermal heating around the cavity through the Joule effect induced by carriers that are swept through the device. This additional deposited power is directly controlled by the current and applied bias. Moreover, the power is deposited at the location where the cavity optical mode is centered. By measuring the spectral shift of the resonance wavelength as a function of the applied bias, we can directly deduce the effective thermal resistance of the cavity without any adjusted parameters. We have performed the measurements on a cavity fabricated on a silicon-on-insulator substrate, but the technique could be applied to any semiconductor cavities.

The investigated samples were fabricated from a silicon-on-insulator substrate with a 2 μm thick buried oxide. The silicon thickness is 200 nm, and the photonic crystal lattice periodicity a is 400 nm. We use a width-modulated line defect cavity following design A1 presented in [12]. The global structure is symmetric and, from left to center, can be described by the following elements: an inverted taper to inject or collect light from lensed fibers, a silicon waveguide, a coupling taper to inject light into a W1.02 photonic crystal waveguide, a tunnel barrier to control the coupling between the W1.02 waveguide and the cavity and the cavity itself. The cavity is designed in a W0.98 photonic crystal waveguide. A Wx waveguide corresponds to a photonic crystal waveguide with a single row of holes missing and a separation distance between hole centers on each side of the waveguide of $\sqrt{3}\,a$ x. The length of the photonic crystal
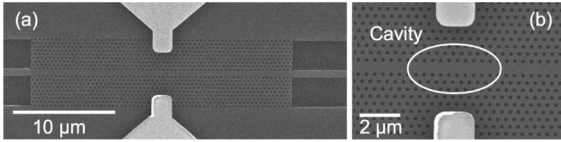
Fig. 1. (a) Scanning electron microscopy image of the studied photonic crystal structure. (b) Zoom around the cavity surrounded by the two metallic pads. The cavity is defined by a width modulation of the waveguide formed by one missing row of air holes. The center of the cavity mode lies between the metal pads.

structure is 25 µm, and the total length of the sample is 500 µm. The buried oxide is not removed. After photonic crystal fabrication using a Nanobeam NB04 electronic lithography system, a second lithography step with the same system is performed in order to deposit the metal contacts close to the cavity. An alignment precision better than 30 nm is achieved. We have chosen platinum as Schottky contacts (200 nm thickness) because of its high Schottky barrier height for electrons. Figure 1(a) shows a scanning electron microscope image of the whole photonic crystal structure, while Fig. 1(b) shows a zoom around the cavity surrounded by the two metal contacts. The resonance wavelength of the cavity is 1538 nm with a quality factor around 40,000. The electrical characteristics of the metal-semiconductor-metal device and its photoresponse are described in detail in [13,14]. Carrier depletion is controlled by the applied bias. More importantly, when applying a bias, the effective free carrier lifetime can be significantly reduced by a factor as large as 50 leading to an effective carrier lifetime in the cavity as small as 10 ps at high applied bias. This property can be used in order to keep a high-quality factor even under strong optical pumping.

Figure 2 shows the dependence of the photocurrent as a function of the input power. As will be shown below, the knowledge of the photocurrent allows one to determine the Joule thermal power deposited in the cavity. The applied bias is 10 V corresponding to a partial depletion of the photonic crystal structure. The lateral width of the depletion region is around 1.5 µm as confirmed by electron beam induced current measurements [14]. The photocurrent I increases regularly as the input power is increased and saturates above 800 µW.
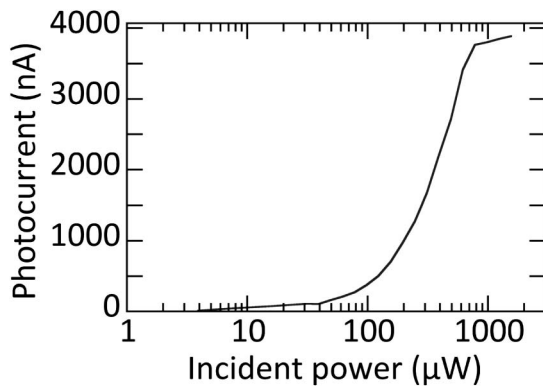
The photocurrent depends on the stored energy in the cavity and on the carriers that are generated either by linear and two-photon absorption as described in [14]. The absorbed power inside the cavity depends on the linear absorption, the two-photon absorption, and on the free carrier absorption. The latter mechanism depends on the effective carrier lifetime in the cavity and is thus difficult to estimate accurately. These mechanisms contribute to the spectral shift of the cavity resonance wavelength as a consequence of free carrier dispersion effect and thermal heating of the cavity. The other source of dissipated power that leads to thermal heating of the cavity is the Joule effect. For a fixed incident optical power on the cavity, we can control the dissipated Joule power by adjusting the applied bias. Figure 3 shows the variation of the output power as a function of the applied bias. The incident optical power is 200 µW. The spectral shapes are asymmetric because of the nonlinear response of the cavity. A clear redshift of the resonance is observed as the bias is increased and results from the competition between the heating of the cavity (redshift) and the free carrier dispersion effect (blueshift). We have modeled the different contributions that lead to the thermal heating of the cavity. The contribution of Joule effect is dominant for powers up to few hundreds of µW, as long as the effective free carrier lifetime is sub-nanosecond, which is the case in the present experiment [14]. However, at small input powers, the free carrier dispersion effect plays a significant role in the blueshift of the resonance, and it is not straightforward to distinguish between the free carrier dispersion effect and thermal heating. In the range between 100 and 700 µW, the dominant source of the spectral shift is due to thermal heating induced by the Joule effect.

Figure 4 shows the resonance shift of the cavity as a function of the input power for different applied bias. In the range of input powers below the saturation of photocurrent and above the regime where the free carrier dispersion effect is significant (below 100 µW), one can deduce the thermal resistance of the cavity from the relative variation of the spectral shift following Eq. (1):

$$\delta\lambda = \frac{\delta n}{n_{Si}}\lambda_0 = \frac{\partial n}{\partial T}\Delta T\frac{\lambda_0}{n_{Si}} = \frac{\partial n}{\partial T}R_{th}P\frac{\lambda_0}{n_{Si}}, \qquad (1)$$

Fig. 2. Photocurrent (nA) as a function of incident power (µW) for a 10 V applied bias. The input power corresponds to the waveguide power in front of the photonic crystal cavity. The pump wavelength is 1538 nm.
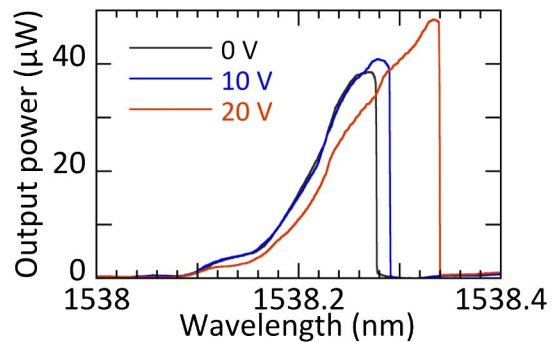
Fig. 3. Output power for different applied bias. The input power is 200 µW. The wavelength is scanned from a short to long wavelength. The output power corresponds to the power in the waveguide at the exit of the photonic crystal cavity.
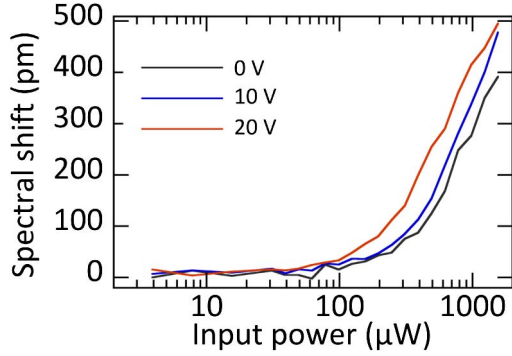
Fig. 4.   Spectral shift deduced from measurements as reported in Fig. 3 for different applied bias as a function of the optical input power. The thermal resistance is deduced from the difference of spectral shift between two applied bias for a fixed optical input power.

where P is the dissipated power and ΔT the effective temperature increase in the structure seen by the optical mode. $n_T = (\partial n/\partial T)$ is the silicon thermo-optic coefficient $(1.87 \times 10^{-4} \text{ K}^{-1})$ [10,15]. The maximum effective temperature increase in the present experiments is around 6 K. At a fixed optical pump power and for two distinct polarizations, V_1 and V_2, the supplemental power dissipated in the cavity δP is due to Joule effect and equals to $I(V_2)V_2 - I(V_1)V_1$. The effective thermal resistance R_{th} can thus be obtained from Eq. (2):

$$\delta\lambda(V_2) - \delta\lambda(V_1) = R_{\text{th}} n_T \frac{\lambda_0}{n_{Si}} (I(V_2)V_2 - I(V_1)V_1). \quad (2)$$

The change in wavelength due to thermal expansion and hole size modification is neglected because of the weak value of silicon thermal expansion coefficient. The main interest of this approach is that it does not depend on the exact knowledge of the optical power locally absorbed and dissipated. Only the knowledge of applied bias and measured current are necessary to extract the thermal resistance from the spectral shift of the resonance wavelength. Moreover, the value is obtained by the difference between two applied bias. It ensures that the contribution from the resistive Joule effect will be the dominant differential source of thermal heating, independently of the dissipated optical power. We have measured the thermal resistance from the spectra presented in Fig. 4 for an input optical power range between 200 and 500 μW. The measured values are comprised between $1.5–1.7 \times 10^4 \text{ KW}^{-1}$ with an average value of $1.6 \times 10^4 \text{ KW}^{-1}$. The thermal resistance value can be compared to those reported in [16,11] and [10] for a membrane-type 2D photonic crystal $(5 \times 10^4 \text{ KW}^{-1}$ and $1.5–3.5 \times 10^4 \text{ KW}^{-1}$, respectively). The lower value reported here results from the presence of the buried oxide, which provides an additional path for energy dissipation as compared to suspended membranes as well as a change in the mode profile.

We have performed a 3D steady-state analysis of the thermal distribution using a finite element solver [17]. It allows us to investigate the temperature profile and power dissipation in the structure. The photonic crystal area was modeled by hole-free material with an effective thermal conductivity of 81.9 $\text{WK}^{-1} \text{m}^{-1}$ [18,19]. This value

was determined by taking into account the photonic crystal pattern and assuming the continuity of thermal flux through the drilled photonic crystal zone. Its value is linked to the air filling factor. A thermal conductivity of 130 $\text{WK}^{-1} \text{m}^{-1}$ was considered for the rest of silicon, i.e., the W1 waveguide and the silicon slab surrounding the photonic crystal area [20]. We have not taken into account the dependence of the thermal conductivity as a function of temperature, since the temperature increase remains small in the Kelvin range. The metallic pads were also considered in the modeling. The size of the modeling volume is 150 μm × 100 μm × 500 μm, where 150 μm represents the dimension along the waveguide direction, 100 μm the direction perpendicular to the waveguide, and 500 μm the dimension along the vertical direction. The heat source resulting from the carrier transport between the pads was simulated by a parallellepipedic zone inserted in the silicon volume between the metallic pads. We have set as boundary conditions a temperature of 293 K at the edge of the structures. Along the waveguide direction, the spatial temperature profile has a full width at half-maximum of about 4 μm. This width directly depends on the anisotropic geometry of the heated zone. The heated volume is thus larger than the one given by the cavity volume. We have checked that this spatial distribution is not dependent on the distance where the boundary conditions are imposed, indicating the 3D nature of heat propagation in this structure. The temperature variation was projected on the cavity mode profile calculated independently by finite difference in time domain modeling. This projection is necessary as the spectral shift of the cavity mode depends on the temperature seen by the optical mode and experimentally corresponds to the response of the system. An effective thermal resistance of $1.27 \times 10^4 \text{ KW}^{-1}$ is obtained by calculation close to the average value experimentally measured $(1.6 \times 10^4 \text{ KW}^{-1})$. If the metallic pads are not considered in the modeling, the thermal resistance increases slightly up to $1.32 \times 10^4 \text{ KW}^{-1}$. In a structure without buried oxide, i.e., for a suspended membrane photonic crystal, the thermal resistance is, as expected, higher up to $1.68 \times 10^4 \text{ KW}^{-1}$. Note that the same mode profile as the one for structures on oxide is considered in this case. We also note that without photonic crystal, i.e., in a silicon slab on oxide and with metallic pads, an equivalent thermal resistance of $1.05 \times 10^4 \text{ KW}^{-1}$ is calculated. It indicates that the air holes increase the thermal resistance by 20%, without accounting for the change in the mode profile. The modeling results are summarized in Table 1. The deviation between modeling and

Table 1.   Comparison Between the Experimental Value (Exp.) and Modeling for the Effective Thermal Resistance (R_{th}) (K/W) for Different Photonic Crystal Configurations[a]

	Exp.	Modeling			
		(a)	(b)	(c)	(d)
R_{th}	16000	10500	12700	13200	16800

[a](a) Without photonic crystal and with metallic pads. (b) Photonic crystal on oxide with metallic pads. (c) Photonic crystal on oxide. (d) Suspended photonic crystal with metallic pads.

experiment (1.27 versus. 1.6×10^4 KW^{-1}) is mainly attributed to the approximation of an homogeneous parallelepiped for the heated zone defined by the metallic contact size and separation between them. Moreover, contact resistance should be considered in more refined modeling. The accuracy of the measurement could be improved by minimizing the free carrier dispersion, i.e., the free carrier density. It could also be improved by increasing the difference of bias, while keeping control of the mechanisms inducing the dispersion. This would imply to move away the metallic pads. The interest of this modeling is twofold: first, it confirms that the presented method is relevant to obtain an experimental value for the thermal resistance of a photonic crystal cavity. Second, it allows us to identify the respective contribution of the different parts of the structures, as the role of the metallic pads and the role of oxide. This information is necessary in order to optimize the design of future structures using the metallic contacts in close proximity with the photonic crystals.

In conclusion, we have shown that the effective thermal resistance of a photonic crystal microcavity can be measured without having to exactly know the absorbed optical power in the cavity. This method illustrates the interest of combining nanophotonics and electrical control of the photonics devices. Moreover, the metallic pads open the possibility to control the free carrier lifetime and photo-induced carrier density, and in turn the free carrier absorption. Thermal heating and *in fine* the thermal resistance can thus be tuned following this approach. The local control of carrier depletion, carrier collection, and on-demand adjustable thermal heating represents interesting perspectives in the field of nonlinear nanophotonics.

References

1. T. Tanabe, M. Notomi, S. Mitsugi, A. Shinya, and E. Kuramochi, Opt. Lett. **30**, 2575 (2005).
2. K. Nozaki, A. Shinya, S. Matsuo, Y. Suzaki, T. Segawa, T. Sato, Y. Kawaguchi, R. Takahashi, and M. Notomi, Nat. Photonics **6**, 248 (2012).
3. B. Corcoran, C. Monat, C. Grillet, D. J. Moss, B. J. Eggleton, T. P. White, L. O'Faolain, and T. F. Krauss, Nat. Photonics **3**, 206 (2009).
4. Y. Akahane, T. Asano, B. S. Song, and S. Noda, Nature **425**, 944 (2003).
5. Z. Han, X. Checoury, D. Neel, S. David, M. El Kurdi, and P. Boucaud, Opt. Commun. **283**, 4387 (2010).
6. H.-G. Park, S.-H. Kim, S.-H. Kwon, Y.-G. Ju, J.-K. Yang, J.-H. Baek, S.-B. Kim, and Y.-H. Lee, Science **305**, 1444 (2004).
7. X. Checoury, Z. Han, and P. Boucaud, Phys. Rev. B **82**, 041308 (2010).
8. N. Cazier, X. Checoury, L.-D. Haret, and P. Boucaud, Opt. Express **21**, 13626 (2013).
9. L.-D. Haret, T. Tanabe, E. Kuramochi, and M. Notomi, Opt. Express **17**, 21108 (2009).
10. P. E. Barclay, K. Srinivasan, and O. Painter, Opt. Express **13**, 801 (2005).
11. T. Uesugi, B. S. Song, T. Asano, and S. Noda, Opt. Express **14**, 377 (2006).
12. E. Kuramochi, M. Notomi, S. Mitsugi, A. Shinya, T. Tanabe, and T. Watanabe, Appl. Phys. Lett. **88**, 041112 (2006).
13. L.-D. Haret, X. Checoury, Z. Han, P. Boucaud, S. Combrié, and A. de Rossi, Opt. Express **18**, 23965 (2010).
14. L.-D. Haret, X. Checoury, F. Bayle, N. Cazier, P. Boucaud, S. Combrié, and A. de Rossi, Opt. Express **21**, 10324 (2013).
15. G. Cocorullo, F. G. Della Corte, and I. Rendina, Appl. Phys. Lett. **74**, 3338 (1999).
16. T. Asano, W. Kunishi, M. Nakamura, B. Song, and S. Noda, Electron. Lett. **41**, 37 (2005).
17. M. Tinker and J.-B. Lee, Opt. Express **13**, 7174 (2005).
18. M. Chahal, G. K. Celler, Y. Jaluria, and W. Jiang, Opt. Express **20**, 4225 (2012).
19. W. Song, M. Chahal, G. K. Celler, Y. Jaluria, G. T. Reed, and W. Jiang, Opt. Express **21**, 4235 (2013).
20. R. G. Morris and J. G. Hust, Phys. Rev. **124**, 1426 (1961).